On Binary *P-T* Phase Diagrams

A. BLOCK-BOLTEN and DONALD R. SADOWAY

A thermodynamic analysis of the concentration and temperature dependencies of oxygen pressure in metal-metal oxide systems is presented. The resulting binary *P-T* phase diagrams show the various species in the context of relative reducibility not only for pure elements and compounds but also for the solutions and intermediate compounds which form. It is not necessary to presume a model for the thermodynamic behavior of solid and/or liquid solutions in this treatment. The Cr-Cr_2O_3 system is presented as an example. Verification is found in the previously reported data on the V_2O_4-V_2O_5 system.

I. INTRODUCTION

THE search for alternative graphical representations of thermodynamic properties in binary and multicomponent systems is not new. Indeed, the method described herein is based upon two independent earlier efforts: those of Darken and Flengas. In their work on the equilibria between iron, oxygen, and various oxides Darken and Gurry displayed the relevant phase boundaries on a plot of $1/T$ *vs* log P_{O_2}.[1] Those who study high temperature corrosion are familiar with such thermal stability plots. However, the temperature range of interest is narrow, and the various species appear as discrete chemical substances.[2] Some twenty years after the Darken and Gurry publication Flengas began analyzing plots of log P *vs* $1/T$ in terms of a series of isopleths or so-called "pressure trees".[3] This approach permits experimental verification in the form of detailed vapor pressure studies on a variety of reactive metal chloride systems.[3-6] Unfortunately, neither treatment was fully exploited by others.

The purpose of the present report is to extend and modify both the Darken and Flengas treatments to demonstrate their application to "mainstream" systems of metallurgical interest. Specifically, the isopleth construction of "pressure trees" is used to make a *binary P-T* phase diagram. In doing so, it must be emphasized that it is not necessary to presume a model for the thermodynamic behavior of the solid and/or liquid solutions which form. Furthermore, binary *P-T* phase diagrams show the reacting species in the context of relative reducibility instead of in the context of state of matter and/or crystallographic modification as in the case of conventional phase diagrams, *i.e.*, *T vs X* plots. From the standpoint of process design and optimization, the two types of phase diagrams (*P-T* and *T-X*) complement one another, each providing vital information.

Brewer and Searcy have examined the behavior of various gaseous species over liquid Al_2O_3 and a mixture of liquid Al and solid Al_2O_3.[7] Knacke and Neumann used a similar approach in the analysis of oxide and sulfide systems of lead and zinc.[8] However, in all cases partial pressures were those in equilibrium with *pure* elements or *pure* compounds.

This article presents as examples the detailed thermodynamic analyses of two oxide systems: Cr-Cr_2O_3 and V_2O_4-V_2O_5, and treats the solutions and intermediate compounds formed by the principal compounds in question.

A. BLOCK-BOLTEN, Research Scientist, Materials Processing Center, and DONALD R. SADOWAY, Associate Professor, Department of Materials Science and Engineering, are both with Massachusetts Institute of Technology, Cambridge, MA 02139.

Manuscript submitted August 31, 1981.

II. THE THERMODYNAMICS OF OXIDE SYSTEMS

A. *The* Cr-Cr_2O_3 *System*

Figure 1 shows the schematic representation of the phase diagram of the Cr-Cr_2O_3 system. This representation follows closely that reported in the literature with the exception of allowing herein for a range of nonstoichiometry in Cr_2O_3.[9,10] The various temperature-composition zones or phase fields have been labeled. Figure 2 shows the complete oxygen pressure plot for the Cr-Cr_2O_3 system. For the most part it is schematic, as there were few data in the literature on the oxygen pressures associated with the various phase equilibria in the system. In the low temperature range below the eutectic, oxygen pressures were estimated by extrapolation of data reported by Mazandarany and Pehlke[11] (see inset of Figure 2).

To explain the derivation of the "pressure trees" of Figure 2, the behavior of several representative solutions will be followed as they are heated through the various phase fields labeled in Figure 1.

Zone I is the region of nonstoichiometry in Cr_2O_3 and, as such, is a solid solution of Cr in Cr_2O_3 designated α. The phases present are O_2 gas and the α solid solution. The equilibrium in this phase field may be written as

$$\frac{2}{3}\underline{Cr_2O_3}(\alpha) = \frac{4}{3}\underline{Cr}(\alpha) + O_2(g) \qquad [1]$$

where the lines under Cr_2O_3 and Cr denote that each is in solution. The free energy change for the reaction is

$$\Delta G = \Delta G^\circ + \frac{4}{3}RT \ln a_{Cr} + RT \ln P_{O_2} - \frac{2}{3}RT \ln a_{Cr_2O_3} \qquad [2]$$

where the activities of Cr and Cr_2O_3 are with respect to the pure solids, and it is assumed that the fugacity of O_2 is equal to its partial pressure. At equilibrium $\Delta G = 0$, and Eq. [2] may be rearranged as

$$RT \ln P_{O_2} = -\Delta G^\circ - \frac{4}{3}RT \ln a_{Cr} + \frac{2}{3}RT \ln a_{Cr_2O_3} \qquad [3]$$

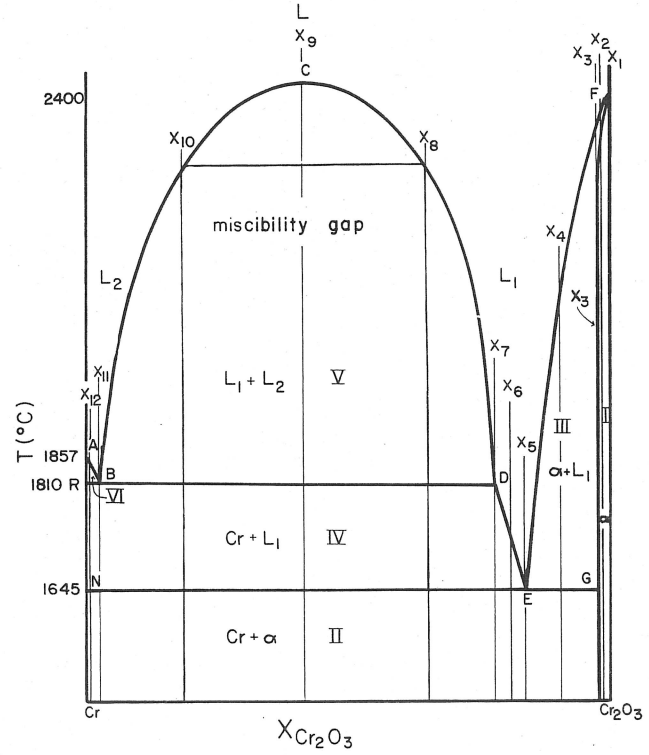

Fig. 1 — Schematic representation of the Cr-Cr_2O_3 phase diagram.

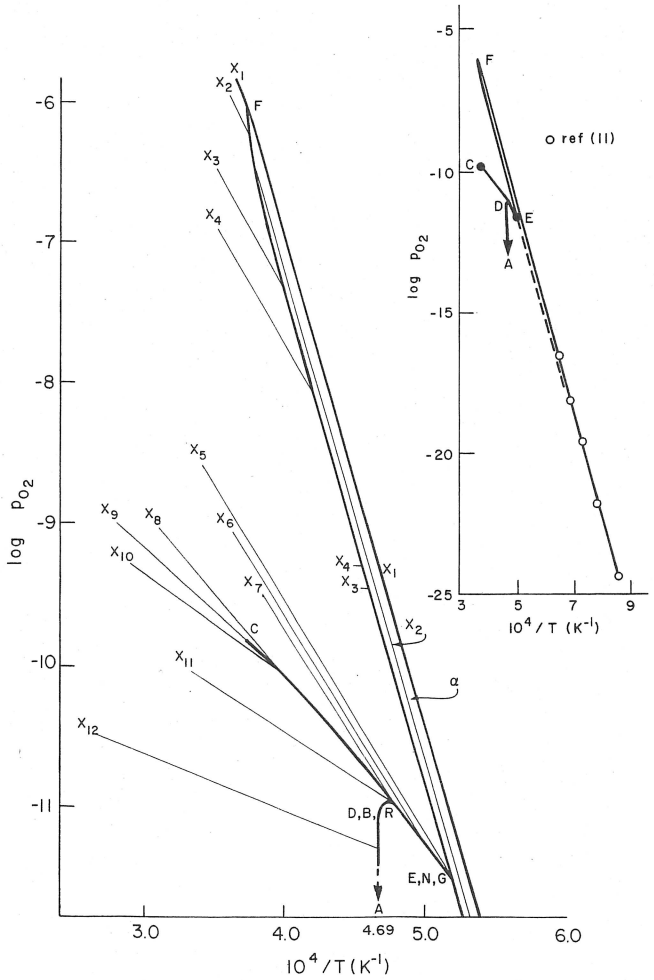

Fig. 2 — Binary *P-T* phase diagram for the Cr-Cr_2O_3 system (schematic).

The temperature dependence of oxygen pressure is then

$$\frac{\partial \ln P_{O_2}}{\partial\, 1/T} = \frac{-\Delta H^\circ - \frac{4}{3}\Delta\overline{H}_{Cr} + \frac{2}{3}\Delta\overline{H}_{Cr_2O_3}}{R} \qquad [4]$$

where ΔH° is the enthalpy of decomposition of pure solid Cr_2O_3 into pure solid Cr and O_2 gas at a pressure of 1 atmosphere (101.325 kPa), and $\Delta\overline{H}_{Cr}$ and $\Delta\overline{H}_{Cr_2O_3}$ are the partial molar enthalpies of mixing of Cr and Cr_2O_3, respectively. If the temperature dependence of ΔC_p is neglected, for a solution of any composition in zone I a plot of log P_{O_2} *vs* $1/T$ should be linear with a slope of $(-\Delta H^\circ - 4/3\ \Delta\overline{H}_{Cr} + 2/3\ \Delta\overline{H}_{Cr_2O_3})/2.3$ R. If ΔC_p is strongly dependent upon temperature, the plot is nonlinear. However, even with pronounced variation in ΔC_p, the degree of curvature can be expected to be slight. From the phase rule, the variance of the system in zone I is 2. Thus, solutions of different compositions should have different equilibrium oxygen pressures. The higher the oxygen content of the solution, *i.e.*, the higher $X_{Cr_2O_3}$, the higher the equilibrium P_{O_2}. If ΔH° is assumed to be large relative to $\Delta\overline{H}_{Cr}$ and $\Delta\overline{H}_{Cr_2O_3}$, in zone I a series of effectively parallel straight lines as shown in Figure 3(b) should represent the oxygen pressure above the solutions as selected in Figure 3(a). Table I summarizes these conclusions.

Zone II is the two-phase region below the eutectic temperature and between pure solid chromium and the α solid solution. In Figure 1 the right-hand boundary has been stylized as being effectively an isopleth. Because the variance of the system in this phase field is unity, specifying the temperature is sufficient to fix the pressure. Thus, at a given temperature any mixture in zone II will have the same oxygen pressure, independent of its composition. Accordingly, the oxygen pressures for the entire range of mixtures of zone II fall on a single curve when plotted as a function of temperature and composition.

Zone L is the all-liquid region where the phases present are oxygen gas and a homogeneous melt of Cr and Cr_2O_3. The variance of the system in zone L is 2; hence, as in zone I, one expects P_{O_2} to be a function of both temperature and composition. For any given concentration the plot of log P_{O_2} *vs* $1/T$ should be linear with a slope of $(-\Delta H^\circ - 4/3\Delta\overline{H}_{Cr} + 2/3\Delta\overline{H}_{Cr_2O_3})/2.3R$, where $\Delta\overline{H}_{Cr}$ and $\Delta\overline{H}_{Cr_2O_3}$ are the partial molar enthalpies of mixing of Cr and Cr_2O_3, respectively, in the molten solutions formed. ΔH° in this case differs from that of Eq. [4]:

$$\Delta H^\circ_{[5]} = \Delta H^\circ_{[4]} + 4/3\ \Delta_{fus}H_{Cr} - 2/3\ \Delta_{fus}H_{Cr_2O_3} \qquad [5]$$

Figure 4 indicates what happens when a solution of composition X_α is heated through zone III. At temperature T_A, a molten solution of Cr-Cr_2O_3 of composition X_{l_A} is in equilibrium with an α-solid solution of composition X_{α_A}. The relative amounts of each phase are given by the lever rule applied along the tie line, $\underline{A}$-$\overline{A}$. As temperature increases from T_A to T_B, the composition of the α-solid solution changes to a greater Cr_2O_3 content. The effect of this shift in oxygen content is to make the log P_{O_2} *vs* $1/T$ plot nonlinear, as shown in Figure 4(b). The previous description of the behavior of solutions in zone I showed that heating at constant composition, X_2, from $\tilde{A}$ to $\overline{B}$ should give a straight line on a plot of log P_{O_2} *vs* $1/T$. Since at T_A, X_{α_A} is at $\overline{A}$ which is lower in oxygen content than $\tilde{A}$, P_{O_2} at $\overline{A}$ must be

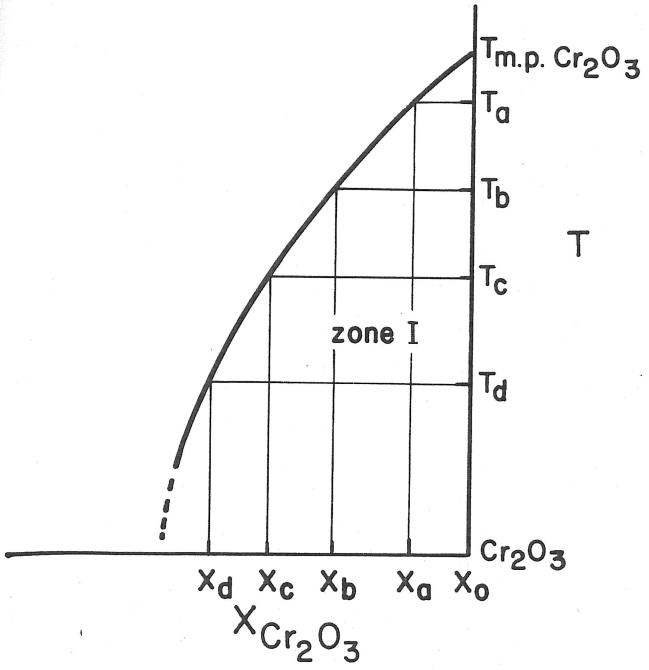

(a)

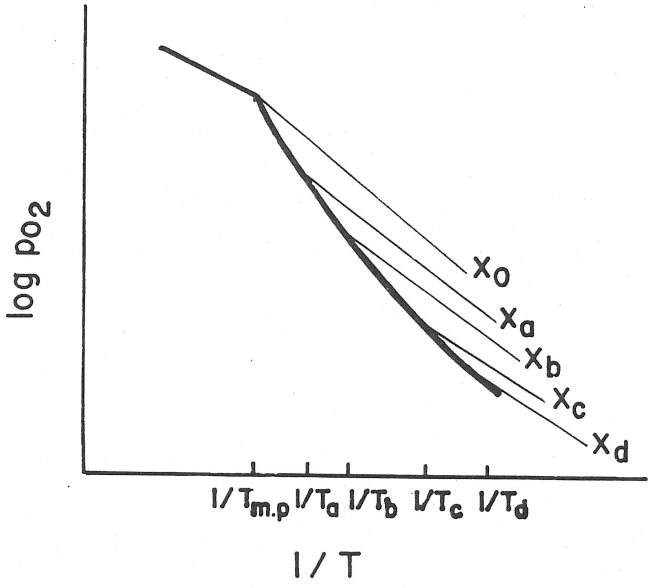

(b)

Fig. 3—(*a*) Phase diagram detail of zone I, (*b*) temperature and concentration dependences of oxygen pressure in zone I.

Table I. Summary of Equilibria in the Cr-Cr_2O_3 System

Zone[1]	Equilibrium[5]	Variance[2]	Curvature[3]	Compositions[4]	Remarks
I	2/3 $\underline{Cr_2O_3}(s) = 4/3\ \underline{Cr}(s) + O_2$	2	linear	X_1, X_2	none
II	2/3 $\underline{Cr_2O_3}(s, \text{sat } \alpha) = 4/3\ \underline{Cr}(s) + O_2$	1	linear provided that $\alpha/(\alpha + Cr)$ boundary is an isopleth	$X_3 \rightarrow X_{12}$	α is the O-rich solid solution of Cr and O which bounds Zone II
III	2/3 $\underline{Cr_2O_3}(l, \text{sat } \alpha) = 4/3\ \underline{Cr}(l) + O_2$	1	positive	X_3, X_4	none
IV	2/3 $\underline{Cr_2O_3}(l) = 4/3\ \underline{Cr}(l, \text{sat pure Cr}(s)) + O_2$	1	negative	$X_6 \rightarrow X_{12}$	degree of curvature depends upon slope of liquidus
V	2/3 $\underline{Cr_2O_3}(l, \text{sat } L_1) = 4/3\ \underline{Cr}(l, \text{sat } L_2) + O_2$	1	negative	$X_8 \rightarrow X_{10}$	curvature governed by shape of O-rich edge of miscibility gap
VI	2/3 $\underline{Cr_2O_3}(l) = 4/3\ \underline{Cr}(l, \text{sat pure Cr}(s)) + O_2$	1	negative	X_{12}	thermodynamically, Zones IV and VI are identical
L	2/3 $\underline{Cr_2O_3}(l) = 4/3\ \underline{Cr}(l) + O_2$	2	linear	$X_1 \rightarrow X_{12}$	none

[1]Zones are defined in Figure 1.
[2]Variance defined by Gibbs phase rule.
[3]Curvature defined as $\partial^2 \log P_{O_2}/\partial(1/T)^2$.
[4]Compositions as labeled in Figure 1.
[5]The notation, "sat α" means "saturated with respect to phase α".

lower there than at $\tilde{A}$ (recall that in zone I the variance is two and P_{O_2} is a function of both temperature and composition). At T_B, the α-solid composition has shifted to higher oxygen content so that its concentration is identical to X_2. Thus, at T_B the oxygen pressures in equilibrium with both solutions must be equal. Figure 4(b) shows this with two curves: the higher pressure straight line belonging to the homogeneous solid solution of composition X_2, and the lower pressure line with positive curvature ($\partial^2 \log P_{O_2}/\partial(1/T)^2 > 0$) that of the α-solid solution which lies on the boundary of zone III. Furthermore, since the variance in zone III is one, all solutions regardless of composition will show the same oxygen pressure dependence on temperature. This is shown in Figure 2 as the common curve GF, which has as its upper limit the congruent melting point of stoichiometric Cr_2O_3.

It is to be noted that GF is deliberately nonlinear. Further justification for not simply connecting points G and F with a straight line is given by Pelton and Schmalzried,[12] who described the general topology of potential *vs* potential diagrams and their relationship to potential *vs* composition diagrams (see Figures 4(a) and 4(b) in Reference 12).

Figure 5 shows what happens when a solution of composition X_8 is heated through zone IV. At temperature T_A a molten solution of Cr and Cr_2O_3 of composition X_{l_A} is in equilibrium with pure solid Cr. As the temperature increases from T_A to T_B, the composition of the melt changes to lower Cr_2O_3 content, *i.e.*, $X_{l_B} < X_{l_A}$. Since the liquid is the only oxygen bearing condensed phase in this case, the shift to lower Cr_2O_3 concentration will control the oxygen pressure in the gas phase so as to make the plot of log P_{O_2} *vs* $1/T$

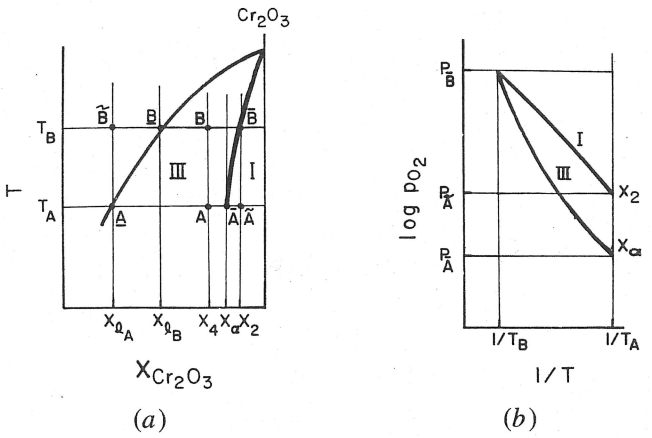

Fig. 4—(*a*) Phase diagram detail of zones I and III, (*b*) temperature and concentration dependences of oxygen pressure in zones I and III.

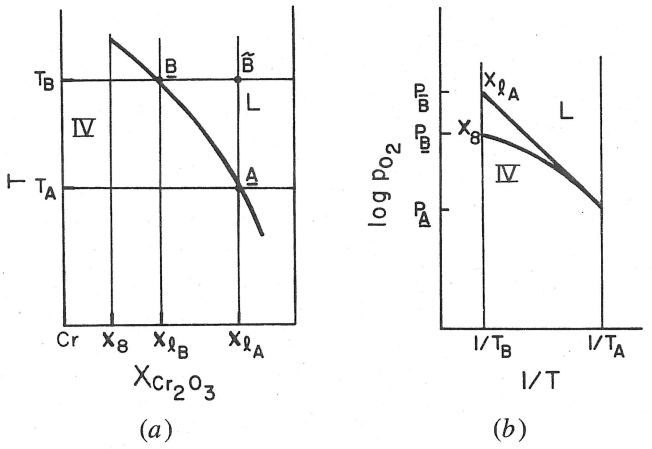

Fig. 5—(*a*) Phase diagram detail of zone IV liquidus, (*b*) temperature and concentration dependences of oxygen pressure in the region of zone IV liquidus.

nonlinear with negative curvature. Figure 5(b) compares the pressure curves for two liquids, both initially of composition X_{l_A} at T_A. One melt is heated at constant composition, X_{l_A}, through zone L. A straight line is expected on a plot of log P_{O_2} *vs* $1/T$. The other melt, which is equilibrated with pure solid Cr, follows the composition of the liquidus. At T_B, $X_{l_B} < X_{l_A}$; thus, P_{O_2} must be lower for the Cr-saturated melt. Accordingly, the plot of log P_{O_2} *vs* $1/T$ for the latter is nonlinear with negative curvature, as shown in Figure 5(b).

Zone V is the miscibility gap. The phases present are oxygen gas and two molten phases, a Cr-rich metal phase and a Cr_2O_3-rich oxide phase. With a variance of 1, oxygen pressure is fixed by temperature alone and is independent of composition along any isotherm. In this sense the situation is similar to zone IV. In both zones the oxygen-rich liquid at the right boundary of the phase field becomes depleted of oxygen as the temperature increases. With the same rationalization given in Figure 5, it is expected that in zone V the oxygen pressure will have negative curvature. In Figure 2 this appears as the segment DC.

When solutions of conjugate composition, such as X_8 and X_{10}, are heated from room temperature, P_{O_2} is expected to be the same for both of them up to the temperature of the boundary of the miscibility gap. At temperatures greater than this, the system is in zone L, the single-phase liquid region. Since $X_{Cr_2O_3}$ is greater for X_8 than for X_{10}, P_{O_2} must be greater above solution 8 than solution 10. In both cases the temperature dependence of P_{O_2} in zone L is linear, the two lines diverging from a common point at the temperature of the boundary of the miscibility gap. The difference in slopes in zone L is related to the difference in the partial molar enthalpies of the two solutions. Furthermore, the very existence of a miscibility gap can be *predicted* from oxygen pressure data. Figure 2 shows that with pressure lines in the all-liquid region tending to intersect at temperatures above the eutectic, a liquid phase miscibility gap must result. Otherwise, below the temperature of intersection the oxygen pressure would be greater over the solution with the lower oxygen content. Instead, below the temperature of intersection the two solutions have a common equilibrium oxygen pressure and thus become conjugates of one another across the miscibility gap at temperatures down to the monotectic. The same predictive capacity applies in the identification of solid phase miscibility gaps.

B. *The* V_2O_4-V_2O_5 *System*

Figure 6 shows a schematic representation of the phase diagram of the V_2O_4-V_2O_5 system.[13,14,15] Figure 7 shows the complete oxygen pressure plot for the system. The diagram integrates data from eight different studies[16–23] to produce

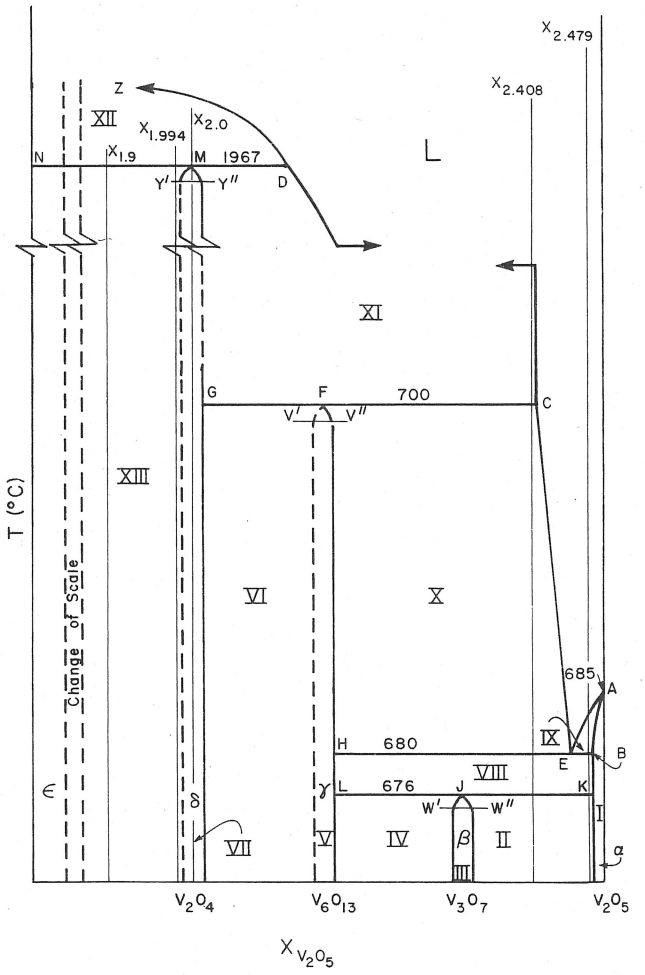

Fig. 6—Schematic representation of the V_2O_4-V_2O_5 phase diagram.

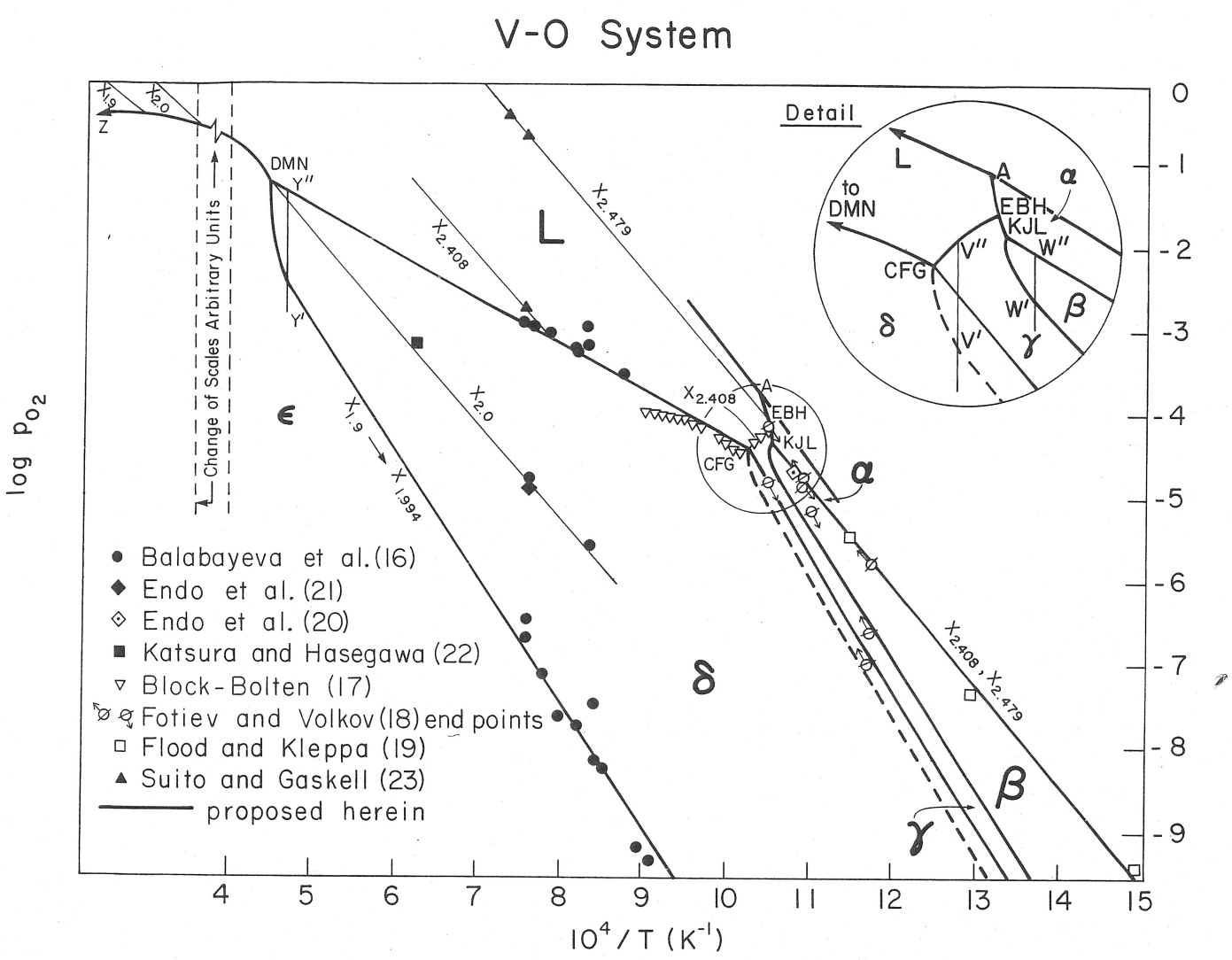

Fig. 7 — Binary *P-T* phase diagram for the V_2O_4-V_2O_5 system (schematic).

a binary *P-T* phase diagram, following the guidelines of isopleth construction presented in Section II-A of this paper. The various solid solution phases have been designated by lower case Greek letters and are defined in Table II which summarizes the relevant chemical equilibria in this system.

Figure 7 shows several characteristics which were not present in the simpler Cr-Cr_2O_3 diagram. For example, zone IV is the two-phase region bounded by the vanadium-rich β-V_3O_7 solid solution and the oxygen-rich γ-V_6O_{13} solid solution. For the most part the phase boundaries do not change composition with temperature. However, as the temperature is raised near the V_3O_7 peritectoid, the right-hand boundary of zone IV changes composition with temperature. In zone IV the variance is one, and at any given temperature there is one oxygen pressure common to all compositions. The equilibrium is

$$4V_3O_7(\beta_{\gamma sat}) = 2V_6O_{13}(\gamma_{\beta sat}) + O_2 \qquad [6]$$

where the solid solutions are saturated with respect to one another. When the composition of the β-V_3O_7 solid solution shifts to higher oxygen content upon heating, the pressure plot shows upward curvature from the low temperature linear behavior in this zone. In this respect the situation is similar to that of zone II in the Cr-Cr_2O_3 system described in greater detail earlier. This is shown in Figure 7, where the oxygen pressure in equilibrium with the γ and β solutions is linear with $1/T$ to W', and then is nonlinear. Solutions spanning the composition interval, W' to J, will be affected in this manner. Another example of such curvature can be found in Figure 3 of Reference 27.

The literature shows V_3O_7 to be tentatively nonstoichiometric.[13,15] This can be verified through the measurement of oxygen pressure in equilibrium with solid V_3O_7 and V_6O_{13}. Linear behavior right up to the V_3O_7 peritectoid would tend to show that this compound is stoichiometric or that deviations from stoichiometry are slight. On the other hand, pronounced curvature would demonstrate a significant range of composition for V_3O_7. The same analysis holds for V_6O_{13} and V_2O_4 in relation to zones VI and XIII, respectively.

In view of the wide ranges of temperature, composition and oxygen potential described, plus the experimental difficulties associated with working with this system, the agreement among the data in Figure 7 and the consistency with the thermodynamic analysis are excellent. Several things are worth noting. Firstly, V_2O_4 is nonstoichiometric and consequently over a very narrow range of composition the oxygen pressure changes dramatically. Figure 7 shows that at

Table II. Summary of Equilibria in the V_2O_4-V_2O_5 System

Zone[1]	Equilibrium[5]	Variance[2]	Curvature[3]	Compositions[4]	Remarks
I	$6\,\underline{V_2O_5}(s) = 4\,\underline{V_3O_7}(s) + O_2$	2	linear	$X_{2.408}, X_{2.479}$	none
II	$6\,\underline{V_2O_5}(s, \text{sat } \beta) = 4\,\underline{V_3O_7}(s, \text{sat } \alpha) + O_2$	1	linear provided that $\alpha/(\alpha + \beta)$ boundary is an isopleth		α and β are the O-rich and V-rich, respectively, solid solutions which bound Zone II
III (a)	$6\,\underline{V_2O_5}(s) = 4\,\underline{V_3O_7}(s) + O_2$	2	linear		none
(b)	$4\,\underline{V_3O_7}(s) = 2\,\underline{V_6O_{13}}(s) + O_2$	2	linear		none
IV	$4\,\underline{V_3O_7}(s, \text{sat } \gamma) = 2\,\underline{V_6O_{13}}(s, \text{sat } \beta) + O_2$	1	linear up to $T_{W'}$, above $T_{W'}$ positive curvature		β and γ are the O-rich and V-rich, respectively, solid solutions which bound Zone IV
V (a)	$4\,\underline{V_3O_7}(s) = 2\,\underline{V_6O_{13}} + O_2$	2	linear		none
(b)	$2\,\underline{V_6O_{13}}(s) = 12\,\underline{VO_2}(s) + O_2$	2	linear		none
VI	$2\,\underline{V_6O_{13}}(s, \text{sat } \delta) = 12\,\underline{VO_2}(s, \text{sat } \gamma) + O_2$	1	linear up to $T_{V'}$, above $T_{V'}$ positive curvature		γ and δ are the O-rich and V-rich, respectively, solid solutions which bound Zone VI
VII (a)	$2\,\underline{V_6O_{13}}(s) = 12\,\underline{VO_2}(s) + O_2$	2	linear	$X_{2.0}$	none
(b)	$14\,\underline{VO_2}(s) = 2\,\underline{V_7O_{13}}(s) + O_2$	2	linear	$X_{1.994}, X_{2.0}$	none
VIII	$3\,\underline{V_2O_5}(s, \text{sat } \gamma) = \underline{V_6O_{13}}(s, \text{sat } \alpha) + O_2$	1	linear provided that $\alpha/(\alpha + \gamma)$ boundary is an isopleth	$X_{2.408}, X_{2.479}$	α, γ defined above
IX	$3\,\underline{V_2O_5}(l, \text{sat } \alpha) = \underline{V_6O_{13}}(l) + O_2$	1	positive	$X_{2.479}$	none
X	$3\,\underline{V_2O_5}(l) = \underline{V_6O_{13}}(l, \text{sat } \gamma) + O_2$	1	negative	$X_{2.408}$	
XI	$2\,\underline{V_2O_5}(l) = 4\,\underline{VO_2}(l, \text{sat } \delta) + O_2$	1	negative	$X_{2.408}$	
XII	$14\,\underline{VO_2}(l) = 2\,\underline{V_7O_{13}}(l, \text{sat } \varepsilon) + O_2$	1	negative	$X_{1.9}, X_{1.994}, X_{2.0}$	ε is the V-rich solid solution which bounds Zone XII
XIII	$14\,\underline{VO_2}(s, \text{sat } \varepsilon) = 2\,\underline{V_7O_{13}}(s, \text{sat } \delta) + O_2$	1	linear up to $T_{Y'}$, above $T_{Y'}$ positive curvature	$X_{1.9}$	ε, δ defined above
L	$2\,\underline{V_2O_5}(l) = 4\,\underline{VO_2}(l) + O_2$	2	linear	all	none

[1]Zones are defined in Figure 6.
[2]Variance defined by Gibbs phase rule.
[3]Curvature defined as $\partial^2 \log P_{O_2}/\partial(1/T)^2$.
[4]Compositions as labeled in Figure 6.
[5]The notation, "sat α" means "saturated with respect to phase α".

1300 K, the oxygen potential spans some four orders of magnitude in the δ region. At the same time, the oxygen pressures measured over two-phase mixtures containing V_2O_4 all lie on a single line regardless of composition. This is shown both for the δ-ε solid-solid phase boundary,[16] and for the δ-liquid phase boundary.[16,17] The data confirm this behavior again in the case of the α-β solid-solid phase boundary.[18,19,20] Secondly, Block-Bolten's data[17] show a relative minimum at the V_6O_{13} peritectic temperature, a feature predicted by the thermodynamic analysis presented herein. Furthermore, the curvature of the oxygen pressure line, EC, between the V_3O_7 peritectoid and V_6O_{13} peritectic temperatures is so negative that over this temperature range oxygen pressure actually *decreases* with increasing temperature. Such behavior has been measured in other systems, such as $NbCl_5$-KCl.[24] On the other hand, at temperatures above the V_6O_{13} peritectic the oxygen pressure increases with temperature while tending toward negative curvature. This suggests that the slope of the liquidus above the V_6O_{13} peritectic temperature is much steeper than below. In other words, above the V_6O_{13} peritectic the increase in pressure due to the increase in temperature is not outweighed by the decrease in pressure due to the shift in the composition of the oxygen-bearing condensed phase to lower oxygen content. Thirdly, the extrapolation of the oxygen pressure line reported by Fotiev and Volkov[18] for the V_6O_{13}-V_2O_4 equilibrium meets Block-Bolten's data[17] at the peritectic temperature. This means that the oxygen-rich boundary of the V_6O_{13}-V_2O_4 two-phase field on Figure 6 (zone VI) must be effectively vertical. In view of this, one wonders whether V_6O_{13} may not be stoichiometric. Fourthly, the extrapolation of the δ-ε and δ-liquid phase boundaries as well as the isopleth at the exact V_2O_4 composition (labeled $X_{2.0}$ in Figure 7) suggests that at the V_2O_4 peritectic temperature, 1967 °C, the oxygen pressure should be approximately 6×10^{-2} atm. Fifthly, data reported by Suito and Gaskell[23] in the all-liquid region are consistent with isopleths derived for the corresponding compositions. Finally, at the congruent melting point of stoichiometric V_2O_5, 685 °C (labeled A on Figures 6 and 7), the oxygen pressure is calculated to be 1.3×10^{-4} atm.[25]

III. CONCLUSIONS

In this article the isopleth construction of "pressure trees" has been used to draw binary *P-T* phase diagrams in two oxide systems of mainstream metallurgical interest. It is

evident from Figures 2 and 7 that the relevant pressure-temperature relationships are nontrivial and are considerably more elaborate than plots of log K_p *vs* $1/T$. The properties of solid and liquid solutions have been described without presumption of any thermodynamic model. The various species are displayed in the context of relative reducibility and thus are particularly useful for process design and optimization.

There are several significant differences between conventional phase diagrams (T *vs* X) and those described herein. For binary systems, conventional phase diagrams display two-phase fields as broad areas, whereas because P_{O_2} varies only with temperature and not composition here, two-phase fields on a pressure plot appear as a single line. On the other hand, single phase fields, particularly nonstoichiometric intermediate compounds which may exist over relatively narrow ranges of composition, appear dwarfed on a conventional phase diagram. On the diagrams described herein, these single phase regions are fully detailed. In fact, the binary P-T diagram for V_2O_4-V_2O_5 (Figure 7) can be viewed as a "patchwork" of single-phase regions, and it is precisely over these single-phase regions that the most dramatic changes in oxygen potential occur. On this basis, the P-T phase diagram can identify potential errors in conventional phase diagrams, such as small ranges of solid compound nonstoichiometry which are often difficult to measure by standard techniques such as cooling curves or DTA (differential thermal analysis). In this respect, in the light of data which can be incomplete and/or conflicting, this plot could be of assistance to those concerned with computer generation of phase diagrams and with the selection of preferred values of thermodynamic properties. As well, the ability to predict the onset of liquid and solid phase miscibility gaps has been described.

P-T phase diagrams minimize the measurements which must be made to characterize a multicomponent system. Oxygen potentials are invariant with respect to composition over broad areas in two-phase fields and vary linearly there with $1/T$. Furthermore, between the all-liquid and two-phase solid regions the oxygen pressure must follow a uniquely defined curve. Thus, a simple eutectic type system with no solid solubility, for example, could be described in considerable detail with oxygen pressure data from just two compositions, one hypereutectic and one hypoeutectic. A vivid example of this is given in the vapor pressure measurements by Kvande in the Na_3AlF_6-Al_2O_3 system.[26] In Reference 26, Figure 2 plots log P *vs* $1/T$. One sees a common line up to 960 °C, the Na_3AlF_6 eutectic. At higher temperatures there are two curves, each of opposite curvature. From these curves emanate linear segments at their respective liquidus temperatures in conformity with the analysis presented herein.

Finally, the treatment can be applied equally well to metal-metal sulfide, metal-metal nitride, and metal-metal halide systems. Adaptation to systems containing more than one volatile component is also possible.

ACKNOWLEDGMENTS

The authors wish to acknowledge the financial support of the Office of Naval Research, Contract No. N000140-C-80-0384 (for A. B.-B.) and the Mining and Mineral Resources Research Institute of the Massachusetts Institute of Technology (for D. R. S.).

REFERENCES

1. L. S. Darken and R. W. Gurry: *J. Amer. Chem. Soc.*, 1946, vol. 68, pp. 798-816.
2. E. Aukrust and A. Muan: *Trans. TMS-AIME*, 1964, vol. 230, pp. 378-82.
3. R. L. Lister and S. N. Flengas: *Can. J. Chem.*, 1965, vol. 43, pp. 2947-69.
4. J. E. Dutrizac and S. N. Flengas: in *Advances in Extractive Metallurgy*, Institution of Mining and Metallurgy, London, 1968, pp. 572-99.
5. D. R. Sadoway and S. N. Flengas: in *Extractive Metallurgy of the Refractory Metals*, H. Y. Sohn, O. N. Carlson, and J. T. Smith, eds., TMS-AIME, Warrendale, PA, 1981, pp. 107-26.
6. S. N. Flengas and A. Block-Bolten: in *Advances in Molten Salt Chemistry*, J. Braunstein, G. Mamantov, and G. P. Smith, eds., Plenum Press, New York, NY, 1973, vol. 2, chap. 2, pp. 27-81.
7. L. Brewer and A. W. Searcy: *J. Am. Chem. Soc.*, 1951, vol. 73, pp. 5308-21.
8. O. Knacke and W. Neumann: *Erzmetall.*, 1956, vol. 9, pp. 261-310.
9. Ya. I. Ol'shanskii and V. K. Shlepov: *Dokl. Akad. Nauk SSSR*, 1953, vol. 91, pp. 561-64.
10. R. E. Johnson and A. Muan: *J. Amer. Ceram. Soc.*, 1968, vol. 51, pp. 430-33.
11. F. N. Mazandarany and R. D. Pehlke: *J. Electrochem. Soc.*, 1974, vol. 121, pp. 711-14.
12. A. D. Pelton and H. Schmalzried: *Metall. Trans.*, 1973, vol. 4, pp. 1395-1404.
13. K. Kosuge: *J. Phys. Chem. Solids*, 1967, vol. 28, pp. 1613-21.
14. S. Kachi and R. Roy: *Second Quarterly Report on Crystal Chemistry Studies*, Pennsylvania State University, University Park, PA, December 4, 1965.
15. A. Burdese: *Ann. Chim. (Roma)*, 1957, vol. 47, pp. 785-96.
16. R. F. Balabayeva, I. A. Vasil'eva, and Ya. I. Gerasimov: *Dokl. Phys. Chem., Proc. Acad. Sci. USSR*, Phys. Chem. Sec., English translation, 1974, vol. 217, pp. 766-69.
17. A. Block-Bolten: *Can. J. Chem.*, 1976, vol. 54, pp. 1967-70.
18. A. A. Fotiev and V. L. Volkov: *Zh. Fiz. Khim.*, 1971, vol. 45, p. 2671.
19. H. Flood and O. J. Kleppa: *J. Amer. Chem. Soc.*, 1947, vol. 69, pp. 998-1002.
20. H. Endo, M. Wakihara, and M. Taniguchi: *Chemistry Letters (Japan)*, 1974, pp. 905-08.
21. H. Endo, M. Wakihara, M. Taniguchi, and T. Katsura: *Bulletin of the Chemical Society of Japan*, 1973, vol. 46, pp. 2087-90.
22. T. Katsura and M. Hasegawa: *Bulletin of the Chemical Society of Japan*, 1967, vol. 40, pp. 561-69.
23. H. Suito and D. R. Gaskell: *Metall. Trans.*, 1971, vol. 2, pp. 3299-3303.
24. D. R. Sadoway and S. N. Flengas: *Can. J. Chem.*, 1978, vol. 56, pp. 2538-45.
25. JANAF Thermochemical Tables, 1975 Supplement, M. W. Chase, J. Curnutt, H. Prophet, R. A. McDonald, and A. N. Syverud, eds., American Chemical Society, Washington, DC, 1975.
26. H. Kvande: *Electrochimica Acta*, 1980, vol. 25, pp. 237-40.
27. T. Matsui and K. Naito: *J. Nucl. Materials*, 1975, vol. 56, pp. 327-35.